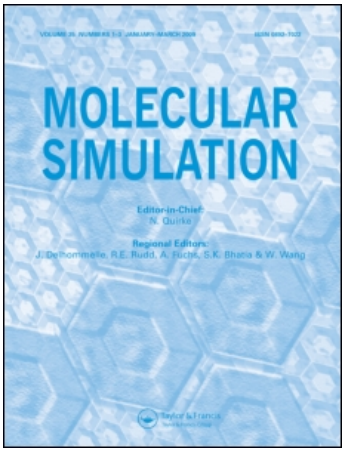

Molecular Simulation
Publication details, including instructions for authors and subscription information:
http://www.informaworld.com/smpp/title~content=t713644482

Equilibrium Molecular Dynamics Computer Simulations of the Transport Coefficients of Ar-CH_4 Mixtures

David M. Heyes[a]; Steve R. Preston[b]
[a] Department of Chemistry, University of Surrey, Guildford, UK [b] Department of Chemistry, Royal Holloway and Bedford New College, University of London, Surrey, UK

To cite this Article Heyes, David M. and Preston, Steve R.(1991) 'Equilibrium Molecular Dynamics Computer Simulations of the Transport Coefficients of Ar-CH_4 Mixtures', Molecular Simulation, 7: 3, 221 — 239
To link to this Article: DOI: 10.1080/08927029108022155
URL: http://dx.doi.org/10.1080/08927029108022155

Molecular Simulation, 1991, Vol. 7, pp. 221–239
Reprints available directly from the publisher
Photocopying permitted by license only

EQUILIBRIUM MOLECULAR DYNAMICS COMPUTER SIMULATIONS OF THE TRANSPORT COEFFICIENTS OF Ar-CH_4 MIXTURES

DAVID M. HEYES

Department of Chemistry, University of Surrey, Guildford, GU2 5XH, UK

STEVE R. PRESTON

Department of Chemistry, Royal Holloway and Bedford New College, University of London, Egham, Surrey, TW20 OEX, UK

(*Received December 1990, accepted January 1991*)

Equilibrium molecular dynamics computer simulations have been used to determine the transport coefficients of model Ar–CH_4 mixtures at state points for which experimental data are available. Both species are represented by single-site Lennard-Jones pair potentials with Lorentz–Berthelot rules for the cross-species interactions. We calculate the self-diffusion coefficients for each species and also mutual-diffusion coefficients using time correlation functions in the Green–Kubo formulae and mean square displacements. Time correlation functions are used to evaluate the shear and bulk moduli and viscosities, thermal conductivity and the thermal diffusion coefficient in [*NVE*] and [*NVT*] ensembles. Only for the bulk viscosity is there a significant ensemble dependence. In order to evaluate the thermo-transport coefficients, we use a rigorous definition for the heat flux, which includes the partial enthalpy of the two species. This was obtained from separate computations carried out at constant pressure in the [*NPT*] ensemble.

The average densities (obtained under [*NPT*] conditions) and thermal conductivities agree well with experiment over a wide temperature and composition range. The simulated shear viscosity of near pure methane is typically ~ 50% higher than experiment. This is seen as a clear shortcoming of a single site model for methane, which fails to account for its orientational properties which appear to be significant for the shear viscosity. The bulk viscosity also shows a similar qualitative discrepancy between experiment and simulation, which we conjecture may be for a different reason. The infinite frequency shear moduli are, in contrast, in very good agreement with experiment.

KEY WORDS: Binary mixtures, argon–methane, MD, partial thermodynamic quantities, transport coefficients, Green–Kubo.

1. INTRODUCTION

Simple fluid mixtures have considerable industrial importance. A ready prediction of their properties, especially their transport coefficients, is therefore of much interest. The prediction of these quantities by analytic theory developed from kinetic theory is still somewhat disappointing. Therefore simulation is, at present, the only reliable analytic bridge between a molecular description of the fluid and its macroscopic transport properties. Although there have been many equilibrium molecular dynamics, MD, studies of transport coefficients in simple fluids and dense liquids using the Green–Kubo time correlation function method, [1] little work of a comprehensive nature has been reported for simple liquid mixtures, despite an ever increasing body

of experimental data. The purpose of the present work is, in part, to redress this imbalance and to apply the Green–Kubo method in MD to *binary* fluid mixtures, with the objective of characterising the density and temperature dependence of their transport coefficients. There has been some work performed on binary mixtures, [2,3] but only at scattered state points and only calculating a limited number of transport coefficients (not always the same ones) at each state point considered. The techniques are now available to determine all the transport coefficients of binary mixtures simultaneously. Although they have not yet been made full use of in any systematic way to build up a body of simulation transport coefficients of the more common mixtures.

In this study we consider model argon–methane mixtures, calculating the self-diffusion, D_i for each component, the mutual diffusion coefficient, D_{12}, [4], the shear viscosity, η_s, [5], the bulk viscoisity, η_B, [6] and thermal conductivity, κ, [7]. We also evaluate the thermal diffusion (the Soret effect) and the diffusion thermoeffect (the Dufour effect), which are numerically identical in the linear response regime according to the Onsager reciprocal relation, D^T, [8]. Although, the small magnitude of D^T and special sensitivity to the integration algorithm for the equations of motion [8] makes them difficult to evaluate with the accuracy we usually expect of simulated transport coefficients ($\pm$ 5%).

Some simulation has also been carried out to determine the thermal conductivity and shear viscosity of model binary mixtures. Evans and Hanley, [9] and Murad [10] computed the shear viscosity of binary Soft-sphere mixtures for several size and mass ratios.

Here we concentrate on liquid Ar–CH_4 state points for which experimental [11] but no simulation data is available. We perform simulations at these experimental state points. Our concern here is not in the mixing rules [12] for the transport coefficients but in the extent to which the MD model can *simultaneously* reproduce the transport coefficients of specific mixtures. Mikhailenko *et al.* [11] determined the bulk and shear viscosity of argon–methane mixtures in the temperature range, 90–140 K, over the full composition range. They investigated the composition and temperature dependence of the shear and bulk viscosities, the shear and bulk infinite frequency moduli, and thermal conductivity. The effect of temperature is quite straightforward for all of these quantities apart from the bulk viscoisity. For fixed composition they decrease with increasing temperature. This is also observed for the bulk viscosity of near-pure methane whereas the reverse trend is manifest for near-pure argon. The composition dependence at fixed temperature is generally more complicated and less easy to predict. In general, in percentage terms, the effect of composition decreases as temperature increases above the triple point temperature of the more 'attractive' component (methane in this case, see Table 1).

An important discovery of Mikhailenko *et al.* [11] was that they found that the shear viscosity increased at constant temperature on going from pure methane to pure

Table 1 Molecular fluid parameters for the Lennard-Jones molecules used in the simulations, taken from ref. [13].

Molecule	m_i/u	ε_{ii}/k_B (K)	σ_{ii}/nm	m_i^*	ε_{ii}^*	σ_{ii}^*
Ar	39.95	119.8	0.3405	1	1	1
CH_4	16.04	152.0	0.374	0.4015	1.26878	1.09838

argon. This is not expected on corresponding states grounds, as the CH_4 has a deeper well-depth than argon. Therefore the CH_4 is at a lower effective reduced temperature, $k_B T/\varepsilon_{CH_4}$, where ε_{CH_4} is the well-depth of the effective pair potential for methane. Our simulations, reported below, demonstrate that the reverse trend is produced if a single site centre model for methane is implemented. In contrast, the thermal conductivity manifests an increase as the mole fraction of Ar, $x_{Ar} \to 0$ at constant temperature, as expected on corresponding states grounds. It is unusual for the thermal conductivity and shear viscosity to have the opposite composition dependence and is not true for Ar–Kr mixtures.

2. THEORY AND SIMULATION METHOD

Fluid Parameters

Both the methane and argon molecules are represented by single centre or site particles. We consider a system of N_1 particles ('molecules') of mass m_1 and N_2 molecules of mass m_2 contained in a volume V, mediated through a Lennard–Jones, LJ, (12–6) potential,

$$\phi_{\mu\nu}(r) = 4\varepsilon_{\mu\nu}((\sigma_{\mu\nu}/r)^{12} - (\sigma_{\mu\nu}/r)^6), \tag{1}$$

where μ and ν are the indices of the two species (i.e., ranging from 1 to 2). The cross-interactions are governed by the generalised mixing rules,

$$\sigma_{12} = (\sigma_{11} + \sigma_{22})/2, \tag{2}$$

and,

$$\varepsilon_{12} = \varepsilon_{11}^{1/2}\, \varepsilon_{22}^{1/2}, \tag{3}$$

These are the Lorentz–Berthelot mixing rules. The MD simulations were performed using cubic unit cells of volume V containing mainly $N = 256$ Lennard–Jones (LJ) particles, although several simulations were conducted with $N = 108$ to assess the N-dependence of the properties. The interactions were truncated at half the box sidelength (S/2). We use both real and LJ reduced units (based on the parameters for species 1, which is Ar) in this report. For example, for temperature, $k_B T/\varepsilon_{11} \to T^*$, and number density, $\rho^* = N\sigma_{11}^3/V$. Reduced time is in units of $\sigma_{11}(m_1/\varepsilon_{11})^{1/2}$, viscosity in $(m_1\varepsilon_{11})^{1/2}/\sigma_{11}^2$, thermal conductivity in $k_B(m_1/\varepsilon_{11})^{-1/2}\sigma_{11}^{-2}$, self-diffusion coefficient in $\sigma_{11}(\varepsilon_{11}/m_1)^{1/2}$ and pressure tensor components in $\varepsilon_{11}\sigma_{11}^{-3}$. The time step, h, was typically ≈ 0.01 in reduced units. In Table 1 we give the LJ and real parameters for the model molecules considered in this work [13]. They are obtained from experimental data on liquids. Also in any study comparing simulation and experiment it is convenient to have interconversion factors to compare real and LJ reduced units. These we give in Table 2. Simulations performed on the CRAY-XMP at ULCC using CFT77 were for typically $\sim 2 \times 10^5$ times steps in production for each state point.

Thermodynamic Properties

The mean configurational energy, U, of the N particles is accumulated as the time average,

$$U = 1/2 \sum_i^N \sum_j^N \phi_{ij} + Nu_{lrc}, \tag{4}$$

Table 2 Conversion factors from reduced to real units, i.e., one combination of reduced units from the second column corresponds to the real units in the third and fourth columns. The reduced units, m, ε and σ are based on Ar, given in table 1.

Quantity	*Reduced units*	*Coefficient*	*Real Units*
Mass, m	m	6.6339	10^{-26}kg mol^{-1}
Time, t	$\sigma m^{1/2}\varepsilon^{1/2}$	2.1564	$10^{-12}s$
Number density, ρ	σ^{-3}	4.2063	10^{-2}mol cm^{-3}
Number density, ρ	σ^{-3}	9.4280	10^{2} Amagat
Number density, ρ	σ^{-3}	1.6804	g cm^{-3}(Ar)
Number density, ρ	σ^{-3}	0.6747	g cm^{-3}(CH_4)
Number density, ρ	σ^{-3}	1.1776	g cm^{-3}(0.5 Ar + 0.5 CH_4)
Volume, V	σ^{3}	23.774	cm^{3}mol^{-1}
Total Energy, E	ε	0.99067	kJ mol^{-1}
Pressure, P	$\varepsilon\sigma^{-3}$	41.898	MPa
Viscosity, η	$m^{1/2}\varepsilon^{1/2}\sigma^{-2}$	0.90349	10^{-4}Pas
Thermal cond., κ	$k_B m^{-1/2}\varepsilon^{1/2}\sigma^{-2}$	1.8803	10^{-2}Jm^{-1}K^{-1}s^{-1}
Diffusion coeff., D	$m^{-1/2}\varepsilon^{1/2}\sigma$	5.3765	10^{-8}m^{2}s^{-1}
ρD	$m^{-1/2}\varepsilon^{1/2}\sigma^{-2}$	1.3619	10^{11}m^{-1}s^{-1}
ρD	$m^{-1/2}\varepsilon^{1/2}\sigma^{-2}$	5.0690	10^{-5}Amagat m^{2}s^{-1}
ρD	$m^{-1/2}\varepsilon^{1/2}\sigma^{-2}$	1.8558 $(T/K)(P/\mathrm{Atm})^{-1}$	10^{-7}atmm^{2}s^{-1}
D^T	$m^{1/2}\varepsilon^{1/2}\sigma^{-2}$	9.0349	10^{-5}m^{-1}s^{-1}kg

Note: k^T is dimensionless. An Amagat is the number density of an ideal gas at 1 atm and 0°C, (ref: Collocot, T.C., and Dobson, A.B., *Dictionary of Science and Technology*, Chambers, 1974.), 1 Amagat $\equiv \rho^* = 1.06067 \times 10^{-3}\sigma^{-3}$.

where $N = N_1 + N_2$. For mole fractions, $x_1 = N_1/N$ and $x_2 = N_2/N$, and partial number densities, $\rho_v = N_v/V = x_v\rho$. The interactions need to be truncated at a separation, $r_c \leqslant S/2$. The long range corrections for $r_{ij} > r_c$ are,

$$u_{lrc} = u^r_{lrc} + u^a_{lrc}, \tag{5}$$

where

$$u^r_{lrc} = \frac{8\pi}{9r_c^9}\left[x_1\varepsilon_{11}\rho_1\sigma_{11}^{12} + 2x_1\varepsilon_{12}\rho_2\sigma_{12}^{12} + x_2\varepsilon_{22}\rho_2\sigma_{22}^{12}\right], \tag{6}$$

and

$$u^a_{lrc} = \frac{-8\pi}{3r_c^3}\left[x_1\varepsilon_{11}\rho_1\sigma_{11}^{6} + 2x_1\varepsilon_{12}\rho_2\sigma_{12}^{6} + x_2\varepsilon_{22}\rho_2\sigma_{22}^{6}\right]. \tag{7}$$

The lower case symbols denote intensive (i.e., per particle) quantities, whereas upper case symbols represent the extensive quantities for the entire system, *e.g.*, $u = U/N + u_{lrc}$. Similarly, the mean enthalpy per particle is $h = H/N$, where

$$H = K_E + U + PV. \tag{8}$$

The kinetic energy per particle, $k_e = K_E/N$ is obtained from,

$$K_E = 1/2\sum_v\sum_i^{N_v}\mathbf{p}_{vi}^2/m_v, \tag{9}$$

where p_{vi} is the momentum of particle i of species v. The instantaneous temperature is,

$$T = 2K_E/(3N - 4)k_B. \tag{10}$$

The temperature and momenta are fixed, resulting in the removal of four degrees of freedom in Equation (10). The pressure is given by,

$$P = \frac{1}{3V}\left[\sum_{v}\sum_{i=1}^{N_v} \mathbf{p}_{vi}^2/m_v - \sum_{i=1}^{N-1}\sum_{j>i}^{N} r\frac{d\phi(r_{ij})}{dr}\right] + P_{lrc}, \tag{11}$$

where the long-range correction to the pressure has a contribution from the repulsive (r) and attractive (a) components of the pair potential,

$$P_{lrc} = P_{lrc}^{r} + P_{lrc}^{a}, \tag{12}$$

where,

$$P_{lrc}^{r} = \frac{32\pi}{9r_c^9}\left[\varepsilon_{11}\rho_1^2\sigma_{11}^{12} + 2\varepsilon_{12}\rho_1\rho_2\sigma_{12}^{12} + \varepsilon_{22}\rho_2^2\sigma^{12}\right], \tag{13}$$

and

$$P_{lrc}^{a} = \frac{-16\pi}{3r_c^3}\left[\varepsilon_{11}\rho_1^2\sigma_{11}^{6} + 2\varepsilon_{12}\rho_1\rho_2\sigma_{12}^{6} + \varepsilon_{22}\rho_2^2\sigma_{22}^{6}\right]. \tag{14}$$

Partial Molar Quantities

Experimental data on partial enthalpies for argon–methane mixtures are not available to use in the simulations of the heat flux, although some experimental data on excess properties of mixing of argon with methane have been measured [14]. Consequently, we undertook separate simulations to determine the partial molar enthalpy and hence (as is revealed in the next section) the exact expression for the heat flux. As we are principally interested in the partial enthalpy we conducted computations in an [NPT] ensemble MD simulation. For intensive property, $y = Y/N$, and mole fractions, x_i we have an m-component mixture the partial thermodynamic quantity,

$$y_i = (\partial y/\partial x_i)_{x_{j,}T,P} \tag{15}$$

From Euler's theorem we can relate the ensemble average thermodynamic quantity, y to these partial derivatives,

$$y = \sum_{i}^{m} x_i y_i. \tag{16}$$

For a binary system this reduces to,

$$y = x_1(\partial y/\partial x_1)_{x_2,T,P} + x_2(\partial y/\partial x_2)_{x_1,T,P}. \tag{17}$$

The total sum of the mole fractions, x is of course,

$$x = \sum_{i}^{m} x_i = 1, \tag{18}$$

If we define,

$$\begin{aligned}\Delta y &= (\partial y/\partial x_1)_{x,\,T,P} \\ &= (\partial y/\partial x_1)_{x_2,T,P} - (\partial y/\partial x_2)_{x_1,T,P} \\ &= y_1 - y_2,\end{aligned} \tag{19}$$

Therefore,

$$y_1 = y + (1 - x_1)\Delta y, \tag{20}$$

and,

$$y_2 = y - x_1 \Delta y. \tag{21}$$

These partial molar quantities have been evaluated for the specific enthalpy, h, and specific volume, $v = V/N$. We used the $[NPT]$ ensemble to determine the partial thermodynamic quantities, using a recently proposed 'particle-swap' method for determining the Δy [15, 16]. Each time step the energy change, ΔU, was evaluated, caused by replacing a particle by one of the other species without altering the configuration. For example, for the two species 1 and 2, the energy change on 'removing' a 1 atom and 'replacing' it by a 2 atom, ΔU^{2+1-},

$$\Delta U^{2+1-} = \sum_{v=1,2}^{2} \sum_{j_v \neq i_1} [\phi_{2v}(r_{i1j_v}) - \phi_{1v}(r_{i1j_v})]. \tag{22}$$

Also,

$$\begin{aligned} \Delta\mu &= \mu_1 - \mu_2 \\ &= \beta^{-1} \ln \langle \exp(-\beta \Delta U^{2+1-}) \rangle_{N_2,N_2} \end{aligned} \tag{23}$$

where $\beta = (k_B T)^{-1}$. In the simulation each particle in turn was chosen every time step as a candidate for this exchange. We also use Widom's particle insertion method to obtain μ_1 and μ_2 directly. If ΔU^{1+} is the energy of a test particle of species 1 randomly inserted in the fluid,

$$\mu_1 = -\beta^{-1} \ln \langle \exp(-\beta \Delta U^{1+}) \rangle_{N_2,T,P,N_1-1}, \tag{24}$$

The transposed expression (i.e., $1 \rightarrow 2$ and $2 \rightarrow 1$ in Equation (24) leads to an expression for μ_2). At every time step, we randomly position N_1 molecules of species 1 and N_2 molecules of species 2 in the fluid. Also,

$$\begin{aligned} \Delta h &= h_1 - h_2 \\ &= -\frac{\langle \Delta U^{2+1-} \exp(-\beta \Delta U^{2+1-}) \rangle_{N_1,N_2}}{\langle \exp(-\beta \Delta U^{2+1-}) \rangle_{N_1,N_2}} \\ &\quad \frac{[\langle H \exp(-\beta \Delta U^{2+1-}) \rangle_{N_1,N_2} - \langle H \rangle_{N_1,N_2} \langle \exp(-\beta \Delta U^{2+1-}) \rangle_{n_1,N_2}]}{\langle \exp(-\beta \Delta U^{2+1-}) \rangle_{N_1,N_2}} \end{aligned} \tag{25}$$

and for the volume,

$$\begin{aligned} \Delta v &= v_1 - v_2 \\ &= \frac{\langle V \exp(-\beta \Delta U^{2+1-}) \rangle_{N_1,N_2}}{\langle \exp(-\beta \Delta U^{2+1-}) \rangle_{N_1,N_2}} - \langle V \rangle_{N_1,N_2}. \end{aligned} \tag{26}$$

The $[NPT]$ equations were introduced in the MD code by box sidelength and velocity rescaling. Constant temperature was achieved approximately using velocity

rescaling procedure in a Verlet leapfrog algorithm [17]. For the desired temperature, T_0 and instantaneous temperature, T, (based on the half-time steps momenta) we determine a momentum rescaling factor,

$$f = (T_0/T)^{1/2}, \tag{27}$$

$$\mathbf{p}(t + h/2) = \mathbf{p}(t - h/2) + \mathbf{F}(t)h. \tag{28}$$

where $\mathbf{F}$ is the systematic force. For each molecule, the new half-timestep velocity is rescaled, $\mathbf{p}(t + h/2) \rightarrow f\mathbf{p}(t + h/2)$. The Anderson constant pressure equations of motion were used to fix a pressure P_0 in the system [18]. This can be rewritten as a series of rescaling operations applied to the molecular co-ordinates and velocities as follows. For a position, r, and momentum, $\mathbf{p}$.

$$\dot{\mathbf{r}} = \mathbf{p} + \dot{\varepsilon}\mathbf{r}, \tag{29}$$

$$\dot{\mathbf{p}} = \mathbf{F} - \varepsilon\dot{\mathbf{p}}, \tag{30}$$

$$\ddot{V} = (P - P_0)/M_A, \tag{31}$$

where the Anderson mass, $M_A = 0.005m_1$, typically.

$$\ddot{\varepsilon} = \frac{\ddot{V}}{3V}. \tag{32}$$

We use the velocity-Verlet algorithm to update the cell volume and implement Equations (29)–(32) in timesteps, h.

$$\dot{V}(t + h/2) = \dot{V}(t - h/2) + \ddot{V}(t)h, \tag{33}$$

$$V(t + h) = V(t) + \dot{V}(t + h/2)h, \tag{34}$$

$$\gamma = [V(t + h)/V(t)]^{1/3} - 1, \tag{35}$$

$$\mathbf{p}(t + h/2) \rightarrow [1 - \gamma]\mathbf{p}(t + h/2), \tag{36}$$

$$\mathbf{r}(t + h) = [1 + \gamma](\mathbf{r}(t) + \mathbf{p}(t + h/2)h). \tag{37}$$

The box sidelength $S = V^{1/3}$ is recalculated each time step to apply the periodic boundary conditions appropriate to the new MD cell dimensions. The long range corrections are also rescaled each time step,

$$u^r_{lrc} = u''^r_{lrc}(S'/S)^{12}, \tag{38}$$

$$u^a_{lrc} = u''^a_{lrc}(S'/S)^6, \tag{39}$$

$$P^r_{lrc} = P''^r_{lrc}(S'/S)^{15}, \tag{40}$$

$$P^a_{lrc} = P''^a_{lrc}(S'/S)^9, \tag{41}$$

where S' is the sidelength used to evaluate reference long range corrections, u''^r_{lrc}, u''^a_{lrc} P''^r_{lrc} and P''^a_{lrc}.

Each time step, the interaction truncation distance is scaled in proportion to S', in order to maintain the same molecules in each $N-$ coordination shells after rescaling.

3. TRANSPORT COEFFICIENTS

In this section we discuss the formulae used to determine the transport coefficients of the system. The [NVT] ensemble was used in the molecular dynamics to determine the transport coefficients. The transport coefficients for a binary mixture of species, $v = 1,2$, can be derived from the microscopically defined fluxes of matter, $\mathbf{J}_v$, and energy, $\mathbf{J}_Q$. Using and adapting the notation of MacGowan and Evans [19],

$$\mathbf{J}_v = N_v m_v(\mathbf{u}_v - \mathbf{u})/V, \tag{42}$$

where from the particle momenta, $\mathbf{p}_i$,

$$\mathbf{u}_v = \frac{1}{N_v m_v}\sum_i^{N_v} \mathbf{p}_i, \tag{43}$$

and,

$$\mathbf{u} = \sum_i^N \mathbf{p}_i/(N_1 m_1 + N_2 m_2). \tag{44}$$

As is conventional in a simulation, $\mathbf{u} = 0$ at the start of the simulation and it does not deviate from this within machine error for the duration of the simulation. Hence, $J_1 = -J_2$ at all time, within machine error ($\sim 1:10^{-12}$).

The heat flux employed in the definition of the transport coefficients thermal conductivity and Soret (Dufour) coefficient, $\mathbf{J}_Q$, is defined as follows,

$$\mathbf{J}_Q = \mathbf{J}_{Q'} - \sum_v \mathbf{J}_v\left[h_v/m_v + \frac{1}{2}(\mathbf{J}_v/m_v\rho_v)^2\right], \tag{45}$$

where h_v is the specific partial enthalpy of species v, evaluated using Equations (20) and (21). The term involving h_v removes from the heat flux, $\mathbf{J}_{Q'}$, the enthalpy flux contribution associated with the interdiffusion of the one species through the other.

$$\mathbf{J}_{Q'} = \frac{1}{2V}\sum_v\sum_{i=1}^{N_v}\left[\{\mathbf{p}_i/m_v - \mathbf{u}\}m_v\{\mathbf{p}_i/m_v - \mathbf{u}\}^2 + \sum_j\{\mathbf{p}_i/m_v - \mathbf{u}\}\cdot(\phi_{ij}\mathbf{l} - \mathbf{q}_{ij}\mathbf{F}_{ij})\right]. \tag{46}$$

The momentum and position of particle i are $\mathbf{q}_i$ and $\mathbf{p}_i$, respectively, $\mathbf{q}_{ij}\mathbf{F}_{ij}$ is the dyad formed out of the two vectors.

The species of v-dependent velocity (v) correlation is,

$$C_{vv} = \frac{1}{3N_v}\sum_{i=1}^{N_v}[\mathbf{p}_i(0)/m_v - \mathbf{u}]\cdot[\mathbf{p}_i(t)/m_v - \mathbf{u}], \tag{47}$$

The self-diffusion for each component is,

$$D_v = \int_0^\infty C_{vv}(t)dt. \tag{48}$$

Time correlation functions were integrated numerically by Simpson's rule to obtain the transport coefficients. As conformation, the D_v were evaluated also using the mean square displacements, $\zeta_v(t)$,

$$\zeta_v(t) = \sum_{i=1}^{N_v}[\mathbf{r}'_i(t) - \mathbf{r}_i(0)]^2/N_v. \tag{49}$$

In this function the particle position, $\mathbf{r}'_i$ are not subjected to periodic boundary condition, PBC, shifts and can take on values outside the MD cell. This is because, from the position of the particle at arbitrary time, $t = 0$, we want to follow it through space as it travels through bulk liquid. The PBC are a mathematical convenience to ensure that in the simulation we concentrate on the same volume of space. (Particles always confined within the MD cell by applications of PBC are denoted by $\mathbf{r}_i(t)$). The self-diffusion for each component is then,

$$D_v = \frac{1}{6}\left[\frac{d\zeta_v(t)}{dt}\right]_{t\to\infty}. \tag{50}$$

The shear viscosity of the mixture is given by the following Green–Kubo relationship,

$$\eta = (V/k_BT)\int_0^\infty \langle P_{\alpha\beta}(0)\, P_{\alpha\beta}(t)\rangle\, dt, \tag{51}$$

where $P_{\alpha\beta}$ is the $\alpha\beta$ ($\alpha \neq \beta$) component of the pressure tensor, $\mathbf{P}$, which is,

$$P_{\alpha\beta} = \frac{1}{V}\left\{\sum_v \sum_{i=1}^{N_v} m_v[p_{\alpha i}/m_v - u_\alpha][p_{\beta i}/m_v - u_\beta] - \sum_{i=1}^{N-1}\sum_{j>i}^{N}(r_{\alpha ij}r_{\beta ij}/r_{ij})\frac{d\phi(r_{ij})}{dr}\right\}, \tag{52}$$

where $r_{\alpha ij}$ is the α Cartesian component of $\mathbf{r}_{ij}$. Equation (52) is simply the m-species generalised formula used in the single component fluids. The theory of elastic moduli in molecular fluids is well described by Zwanzig and Mountain [20]. The infinite frequency shear modulus of the mixture is given by the following fluctuation expression,

$$G_\infty = (V/k_BT)\,\langle P_{\alpha\beta}(0)\rangle^2, \tag{53}$$

The bulk viscosity of the mixture is given by the following Green-Kubo relationship,

$$\eta_B = (V/3k_BT)\int_0^\infty \langle (P(t) - \langle P\rangle)(P(0) - \langle P\rangle)\rangle\, dt, \tag{54}$$

The bulk modulus combination, $K_\infty - K_0$, of the mixture is given by the following fluctuation expression,

$$K_\infty - K_0 = (V/3k_BT) < (P - \langle P\rangle)^2, \tag{55}$$

The value of this quantity will depend on the ensemble used to carry out the simulations. Here we employ $[NVE]$ and $[NVT]$ dynamics for all these quantities. At constant E, the adiabatic zero frequency bulk modulus K_0 will appear in Equation (55). At constant temperature, the isothermal bulk modulus will be the appropriate quantity. Quantities of current interest are the ratio of bulk to shear viscosity, η_B/η and the corresponding ratios if the moduli $G_\infty/(K_\infty - K_0)$. These in turn lead to the phenomenological relaxation times, $\tau = \eta/G_\infty$ and $\tau_B = \eta_B/(K_\infty - K_0)$ which characterise the viscoelastic responses of shear and volume distortions, respectively.

The thermal conductivity, κ is computed from,

$$\kappa = (V/k_BT^2)\int_0^\infty \langle J_{Q\alpha}(0)J_{Q\alpha}(t)\rangle\, dt, \tag{56}$$

where $J_{Q\alpha}$ is the α component of the heat flux, $\mathbf{J}_Q$. If we neglect the last term in

Equation (45) as being insignificant (see the discussion) and let $a = -h_1/m_1$ and $b = -h_2/m_2$ then from (45) and (56) we can calculate three components of κ each determined by a different time correlation function,

$$\kappa = \kappa_{Q'Q'} + \kappa_{Q'J} + \kappa_{JJ}, \tag{57}$$

where,

$$\kappa_{Q'Q'} = (V/k_BT^2) \int_0^\infty \langle J_{Q'\alpha}(0) J_{Q'\alpha}(t) \rangle \, dt, \tag{58}$$

$$\kappa_{Q'J} = (2(a - b)V/k_BT^2) \int_0^\infty \langle J_{Q'\alpha}(0) J_{1\alpha}(t) \rangle \, dt, \tag{59}$$

$$\kappa_{JJ} = [(a - b)^2 V/k_BT^2] \int_0^\infty \langle J_{1\alpha}(0) J_{1\alpha}(t) \rangle \, dt, \tag{60}$$

making use of $J_1 = -J_2$. We see that as $a \to b$ the terms $\kappa_{Q'J}$, (63) and κ_{JJ}, (59) tend to zero. Therefore the formula for the single component fluid is recovered. Equation (62) only remains, being the m-species generalised expression for the single component fluid.

The Soret, $\langle J_Q J_v \rangle$ and Dufour, $\langle J_v J_Q \rangle$ thermal diffusion coefficients are derived from,

$$D_s^T = \frac{V}{k_BT} \int_0^\infty \langle J_{Q\alpha}(0) J_{v\alpha}(t) \rangle \, dt, \tag{63}$$

$$D_D^T = \frac{V}{k_BT} \int_0^\infty \langle J_{v\alpha}(0) J_{Q\alpha}(t) \rangle \, dt, \tag{64}$$

By the principle of microscopic reversibility, $D_s^T = D_D^T$, which we simply denote by D^T here. Separating Equation (64) into the heat flux components as for κ we obtain,

$$D_s^T = D_{sQ'J}^T + D_{sJJ}^T, \tag{65}$$

where,

$$D_{sQ'J}^T = \frac{V}{k_BT} \int_0^\infty \langle J_{Q'\alpha}(0) J_{v\alpha}(t) \rangle \, dt, \tag{66}$$

$$D_{sJJ}^T = \frac{(a - b)V}{k_BT} \int_0^\infty \langle J_{v\alpha}(0) J_{v\alpha}(t) \rangle \, dt. \tag{67}$$

Equations of the same form apply for the decomposition of the Dufour coefficient, with Q' and J simply permuted.

The mutual diffusion coefficient, D_{12}, just as for D_v, can be calculated from a correlation function or an equivalent mean square displacement. We use both routes as a consistency check on the numerical computations.

$$Q^{-1} = 1 + \frac{\rho_1 \rho_2}{(\rho_1 + \rho_2)} (G_{11} + G_{22} - 2G_{12}), \tag{68}$$

where if $g_{v\mu}(r)$ is the species component pair radial distribution function,

$$G_{v\mu} = 4\pi \int_0^\infty r^2 \, dr(g_{v\mu}(r) - 1), \tag{69}$$

evaluated here using Simpson's rule. If,

$$\omega_v = N_v m_v/(N_1 m_1 + N_2 m_2), \tag{70}$$

then,

$$D_{12} = \frac{QV^2}{3Nm_1 m_2 \omega_1 \omega_2} \int_0^\infty \langle J_1(0) J_1(t) \rangle \, dt. \tag{71}$$

An alternative form for D_{12} is from the average square of the distance that the centre of mass of species v particles moves in time t,

$$\zeta_v^{cm}(t) = \sum_{i=1}^{N_v} [\mathbf{r}_v^{cm}(t) - \mathbf{r}_v^{cm}(0)]^2, \tag{72}$$

where,

$$r_v^{cm} = \sum_{i=1}^{N_v} \mathbf{r}_i/N_v, \tag{73}$$

from which,

$$D_{12} = \frac{Q}{6Nm_1 m_2 \omega_1 \omega_2} \left[\frac{d\zeta_v^{cm}(t)}{dt} \right]_{t \to \infty}. \tag{74}$$

From D_T and D_{12} we can define a dimensionless quantity, *thermal diffusion ratio*, k_T, as a measure of the relative importance of thermal and inter-diffusion,

$$k_T = c\left[\frac{D^T}{D_{12}}\right], \tag{75}$$

where,

$$c = \frac{\rho_1 m_1 + \rho_2 m_2}{\rho^2 m_1 m_2}, \tag{76}$$

The value of c is somewhat arbitrary. The above choice is the same as that of Hirschfelder *et al.* [21].

4. RESULTS AND DISCUSSION

Both equilibrium [22,23] and non-equilibrium molecular dynamics [24] 5-site models of methane have been reported. The assumptions inherent in this work and experiment analysis [25–28] is that methane behaves like a noble gas fluid and can consequently be accounted for in its thermophysical behaviour using an effective hard-sphere treatment. The thermal conductivity of methane at room temperature and at pressures up to 35 MPa has been measured [29]. There has also been some experimental work on the transport coefficients of substituted methanes [30]. Mixing laws are now well-developed but not simple [31,32].

Table 3 Thermodynamic quantities of the model liquid Ar–CH_4 mixtures at 1 Atm pressure in reduced units. The specific average enthalpies and chemical potentials of the two species from Equation (24) are given.

N	x_1	N_1	ρ	T^*	h^*	μ_1^*	μ_2^*
256	0.02344	6	0.65382	0.83472	−6.67	−3.40	−5.74
256	0.20312	52	0.67596	0.83472	−6.26	−3.71	−5.71
256	0.39844	102	0.70162	0.83472	−5.81	−3.89	−5.33
108	0.60185	65	0.73387	0.83472	−5.38	−3.74	−5.53
256	0.60156	154	0.72954	0.83472	−5.33	−3.90	−5.42
256	0.79687	204	0.75665	0.83472	−4.85	−3.88	−5.54
256	0.97656	250	0.78169	0.83472	−4.40	−3.88	−5.77
256	0.02344	6	0.61042	1.0017	−5.77	−3.32	−5.09
256	0.20312	52	0.62810	1.0017	−5.36	−3.41	−5.06
256	0.39844	102	0.64744	1.0017	−4.90	−3.40	−5.14
108	0.60185	65	0.67039	1.0017	−4.45	−3.41	−5.12
256	0.60156	154	0.66746	1.0017	−4.41	−3.44	−5.19
256	0.79687	204	0.68459	1.0017	−3.92	−3.46	−5.13
256	0.97656	250	0.69710	1.0017	−3.45	−3.49	−5.19

Most of our simulations were conducted at zero applied pressure along two isotherms for variable Ar/CH_4 compositions. The two temperatures concentrated upon were $T = 100$ K and $T = 120$ K. (In LJ Ar reduced units, using the parameters from Table 1, these correspond to $T^* = 0.83472$ and $T^* = 1.0017$, respectively.)

Summaries of the state points considered and derived thermodynamic quantities from $[NPT]$ simulations are given in Table 3. This table incorporates the average enthalpy per particle and the species-resolved chemical potentials. In order to assess the N-dependence simulations were conducted using $N = 108$ rather than the default number of $N = 256$. A near equimolar mixture ($x_{Ar} = 0.6$) does show a $\sim 1 - 2\%$ N-dependence for the enthalpy and chemical potential, which is satisfactory for most purposes. Therefore as $N = 256$ is adequate for the thermodynamic and transport coefficients we adopt $N = 256$ in most of our simulations. The corresponding partial quantities y_i for enthalpy and volume are given in Table 4. They are as statistically

Table 4 Partial Mixing Properties of model liquid Ar–CH_4 mixtures at 1 Atm pressure by simulation in reduced units. The partial enthalpies are obtained using $[NPT]$ dynamics and Equations (20) and (21).

N	x_1	N_1	ρ^*	T^*	h_1^*	h_2^*	v_1^*	v_2^*
256	0.02344	6	0.65382	0.83472	−4.40	−6.72	1.28	1.54
256	0.20312	52	0.67596	0.83472	−4.35	−6.74	1.28	1.53
256	0.39844	102	0.70162	0.83472	−4.50	−6.67	1.25	1.54
108	0.60185	65	0.73387	0.83472	−4.42	−6.84	1.27	1.51
256	0.60156	154	0.72954	0.83472	−4.23	−6.99	1.26	1.55
256	0.79687	204	0.75665	0.83472	−4.36	−6.79	1.27	1.51
256	0.97656	250	0.78169	0.83472	−4.34	−6.91	1.27	1.49
256	0.02344	6	0.61042	1.0017	−3.69	−5.82	1.36	1.65
256	0.20312	52	0.62810	1.0017	−3.61	−5.80	1.38	1.65
256	0.39844	102	0.64744	1.0017	−3.52	−5.81	1.40	1.64
108	0.60185	65	0.67039	1.0017	−3.44	−5.98	1.42	1.61
256	0.60156	154	0.66746	1.0017	−3.47	−5.83	1.40	1.65
256	0.79687	204	0.68459	1.0017	−3.40	−5.96	1.43	1.59
256	0.97656	250	0.69710	1.0017	−3.38	−6.12	1.43	1.54

Table 5 Comparison of the simulated and experimental densities and shear viscosities. The statistical uncertainty is ± 5 %. All calculations were carried out at constant temperature, in the [*NVT*] ensemble, except the rows denoted by † which denote [*NVE*] ensemble simulations. $N = 256$. We use $\rho/(\mathrm{gcm}^{-3}) = \rho^*(1.6804 \times x_{\mathrm{Ar}} + 0.6747 \times (1 - x_{\mathrm{Ar}}))$ and $\eta_s/(10^{-4}Pas) = 0.90349 \times \eta_s^*$. *denotes a simulation with $r_c^* = 2.5$.

x_{Ar}	ρ^*	T^*	ρ_{sim} $g\,cm^{-3}$	ρ_{exp} $g\,cm^{-3}$	$\eta_s(sim)$ $10^{-4}\,Pas$	$\eta_s expt$ $10^{-4}\,Pas$
0.02344	0.65382	0.83472	0.4565	0.439	2.29	1.54
0.02344	0.65382	0.85940	0.4565	0.439	2.20	1.54†
0.20312	0.67596	0.82593	0.5492	0.590	2.18	1.73†
0.39844	0.70162	0.83472	0.7545	0.752	2.15	1.67
0.39844	0.70162	0.85513	0.7545	0.752	2.05	1.67†
0.39844	0.70162	0.83472	0.7545	0.752	1.99	1.67
0.60156	0.72954	0.83472	0.9336	0.925	1.95	1.69
0.60156	0.72954	0.83210	0.9336	0.925	2.00	1.69†
0.79687	0.75665	0.83472	1.1169	1.106	1.88	1.76
0.97656	0.78169	0.83472	1.2951	1.312	1.81	1.82
0.97656	0.78169	0.82855	1.2951	1.312	1.84	1.82†
0.02344	0.61042	1.0017	0.40219	0.411	1.19	0.98
0.02344	0.61042	0.9719	0.40219	0.411	1.17	0.98†
0.39844	0.64744	1.0017	0.6963	0.688	1.20	1.03
0.39844	0.64744	1.0341	0.6963	0.688	1.21	1.03†
*0.39844	0.64744	1.0330	0.6963	0.688	1.24	1.03†
0.60156	0.66746	1.0017	0.8541	0.837	1.26	1.02
0.60156	0.66746	1.0017	0.8541	0.837	0.74	1.02†
0.97656	0.69710	1.0017	1.1550	1.160	1.10	1.13
0.97656	0.69710	1.0015	1.1550	1.160	1.12	1.13†

well-defined and N-independent as the thermodynamic averages given in Table 3 obtained from the same computations. This is a major advance in technique, that now derivative properties such as the partial quantities calculated here, can be obtained with almost the same statistical uncertainty as the corresponding ensemble averages. Table 4 reveals that partial quantities are significantly less sensitive to composition than the average ensemble quantities (such as energy and enthalpy).

The present LJ model accounts exceptionally well for the density of the mixtures at arbitrary composition, and also for the effects of temperature on the density at fixed composition. The essentially exact agreement between experiment [11] and simulation is demonstrated in Table 5. The density increases as $x_{\mathrm{Ar}} \to 1$ and on decreasing the

Table 6 Comparison of the simulated and experimental densities and shear viscosities of pure methane. The statistical uncertainty is ± 5 %. All calculations were carried out at constant temperature, in the [*NVT*] ensemble, except the rows denoted by † which denote [*NVE*] ensemble simulations. $N = 256$. We use $\rho/(\mathrm{gcm}^{-3}) = 0.6747\,\rho^*$ and $\eta_s/(10^{-4}\mathrm{Pas}) = 0.90349 \times \eta_s^*$.

ρ^*	P MPa	T K	ρ_{sim} mol/l	ρ_{exp} mol/l	$\eta_s(sim)$ $10^{-4}\,Pas$	$\eta_s expt$ $10^{-4}\,Pas$
0.2774	24.2	300	11.67	11.6	0.21	0.22
0.2774†	24.2	292	11.67	11.6	0.235	0.22
0.30223	27.52	300	12.71	12.56	0.253	0.23
0.30223†	26.91	300	12.71	12.56	0.244	0.23
0.67821	27.67	100	28.53	28.47	3.08	2.12
0.67821†	32.40	102	28.53	28.47	3.47	2.12
0.64591	29.27	120	27.17	27.18	1.70	1.36
0.64591†	32.78	122	27.17	27.18	1.80	1.36

Table 7 The simulated properties of pure methane. The statistical uncertainty is ± 5%. All calculations were carried out at constant temperature, in the [*NVT*] ensemble, except the rows denoted by † which denote [*NVE*] ensemble simulations. $N = 256$.

P *MPa*	ρ *mol/l*	T *K*	G_{x_z} *GPa*	$K_{x_z} - K_0$ *GPa*	η_B 10^{-4} *Pas*	κ $10^{-2} Jm^{-1}K^{-1}s^{-1}$	ρ^D $10^{11} m^{-1}s^{-1}$
24.2	11.67	300	0.180	0.240	0.13	0.61	–
24.2 †	11.67	292	0.175	0.188	0.11	0.59	–
27.52	12.71	300	0.222	0.288	0.12	5.64	0.433
26.91 †	12.71	300	0.214	0.255	0.14	5.57	0.429
27.67	28.53	100	1.153	1.029	2.58	21.30	0.0279
32.40 †	28.53	102	1.200	0.499	0.79	20.83	0.0293
29.27	27.17	120	1.024	1.029	1.71	19.99	0.0541
32.78 †	27.17	122	1.061	0.538	0.50	21.06	0.0553

temperature. Graphical display of this data reveals that there is an essentially linear relationship between the densitities of the liquids between the extremes of pure CH_4 and Ar.

Also in Table 5 we compare the experimental and simulation shear viscosities. In the pure argon limit there is, within a statistical uncertainty of ± 5%, agreement between the simulation and experimental values for η_s. For pure argon both simulation and theory agree. However, the composition dependence for $x_{CH_4} \to 1$ is the opposite for simulation and experiment. The experimental values for the shear

Table 8 Comparison of the simulated and experimental mixture bulk viscosities and thermal conductivities. The statistical uncertainty is ± 5%. All calculations were carried out at constant temperature, in the [*NVT*] ensemble, except the rows denoted by † which denote [*NVE*] ensemble simulations. $N = 256$. We use $\kappa/(10^{-2}\mathrm{Jm^{-1}K^{-1}s^{-1}}) = 1.8803\kappa^*$ and $\eta_s/(10^{-4}\mathrm{Pas}) = 0.90349 \times \eta_s$. *denotes a [*NVE*] simulation with $r_c^* = 2.5$.

x_{Ar}	ρ^*	T^*	$\eta_B(sim)$ 10^{-4} *Pas*	$\eta_B(exp)$ 10^{-4} *Pas*	$\kappa(sim)$ $10^{-1} Jm^{-1}K^{-1}s^{-1}$	$\kappa(exp)$
0.02344	0.65382	0.83472	2.05	1.43	1.97	2.09
0.02344	0.65382	0.83472	0.80	1.43	1.93	2.09 †
0.20312	0.67596	0.82593	0.72	1.21	1.65	1.68 †
0.39844	0.70162	0.83472	2.02	1.30	1.38	1.43
0.39844	0.70162	0.85513	0.73	1.30	1.51	1.43 †
0.39844	0.70162	0.83472	1.76	1.30	1.36	1.43
0.60156	0.72954	0.83472	1.55	1.36	1.17	1.28
0.60156	0.72954	0.83210	0.81	1.36	1.16	1.28 †
0.79687	0.75665	0.83472	1.85	1.45	1.20	1.18
0.97656	0.78169	0.83472	1.56	1.57	1.12	1.08
0.97656	0.78169	0.82855	0.92	1.57	1.05	1.08 †
0.02344	0.61042	1.0017	1.27	1.08	1.58	1.72
0.02344	0.61042	0.9719	0.51	1.08	1.51	1.72 †
0.02344	0.61042	0.9719	0.49	1.08	1.87	1.72 †
0.39844	0.64744	1.0017	1.29	1.09	1.13	1.20
0.39844	0.64744	1.0341	0.67	1.09	1.29	1.20 †
*0.39844	0.64744	1.0330	0.57	1.09	1.20	1.20 †
0.60156	0.66746	1.0017	1.18	1.35	0.96	1.05
0.60156	0.66746	1.0017	0.74	1.35	0.99	1.05 †
0.97656	0.69710	1.0017	1.19	1.67	0.83	0.83
0.97656	0.69710	1.0015	1.07	1.67	0.76	0.83 †

Table 9 Elastic moduli of model binary mixtures of model LJ Ar – CH_4 reduced units. The statistical uncertainty is ± 5%. All calculations were carried out at constant temperature, in the [*NVT*] ensemble, except the rows denoted by † which denote [*NVE*] ensemble simulations. $N = 256$. *denotes a [*NVE*] simulation with $r_c = 2.5$. $G_\infty/GPa = 0.041898 \times G^*_\infty$

x_1	ρ^*	T^*	G^*_∞	$G_\infty(sim)$ *GPa*	$G_\infty(exp)$ *GPa*	$K^*_\infty - K^*_0(sim)$
0.02344	0.65382	0.83472	23.86	1.00	1.03	23.32
0.02344	0.65382	0.85940	24.86	1.04	1.03	12.25†
0.20312	0.67596	0.82593	23.11	0.968	0.97	11.67†
0.39844	0.70162	0.83472	22.84	0.957	0.92	23.44
0.39844	0.70162	0.85513	23.35	0.978	0.92	12.50†
0.39844	0.70162	0.83472	22.51	0.943	0.92	23.21
0.60156	0.72954	0.83472	21.92	0.918	0.87	22.82
0.60156	0.72954	0.83210	21.68	0.908	0.87	12.32†
0.79687	0.75665	0.83472	20.74	0.869	0.83	23.07
0.97656	0.78169	0.83472	20.23	0.848	0.80	21.70
0.97656	0.78169	0.82855	19.67	0.824	0.80	12.72†
0.02344	0.61042	1.0017	20.19	0.846	0.88	21.96
0.02344	0.61042	0.9719	19.18	0.804	0.88	11.86†
0.02344	0.61042	1.0822	22.25	0.932	0.88	13.73†
0.39844	0.64744	1.0017	18.55	0.777	0.75	21.48
0.39844	0.64744	1.0341	19.64	0.823	0.75	12.99†
*0.39844	0.64744	1.0330	19.54	0.819	0.75	13.16†
0.60156	0.66746	1.0017	17.55	0.735	0.66	21.02
0.60156	0.66746	1.0017	17.77	0.745	0.66	12.62†
0.97656	0.69710	1.0017	15.29	0.641	0.59	19.00
0.97656	0.69710	1.0015	15.44	0.647	0.59	12.70.†

viscosity decrease as the methane content increases. While the simulation viscosities show the opposite trend. This we believe is not an artefact of experiment or simulation because simulations performed on pure methane presented in Table 6 and Table 7 show similar differences with other independent work. The simulation viscosities of the pure methane are larger than the experimental values of Diller in the liquid state by ~ 50%. Only in the gas phase is there acceptable agreement and a quasi-hard sphere model for methane would appear tenable. This discrepancy is intriguing because another property, the molar volume in experiment and simulation is in excellent concordance. It is tempting to speculate that effective hard-sphere cross-section to shear or orientation motion is lower than that for other properties in which dilation and compressional motion is more important. This has the effect of lowering the shear viscosity below the corresponding states value.

To determine the ensemble dependence of the transport coefficients, we considered [*NVE*] and [*NVT*] ensembles. Table 5 for shear viscosity and Table 8 for bulk viscosity reveals that the only transport coefficient manifesting a significant ensemble dependence is the bulk viscosity. The [*NVE*] values are smaller, largely due to a smaller $K_\infty - K_0$ in the [*NVE*] case rather than at [*NVT*]. At constant E the relevant zero frequency modulus, K_0 is the adiabatic quantity, whereas at constant temperature we have the isothermal K_0. With both isothermal and isoenergetic simulations the bulk viscosity decreases with increasing argon content in the mixture, the opposite trend to experiment. This trend has been also observed for comparable Ar–Kr mixtures [33]. The constant temperature bulk viscosities give closer agreement with the experimental values than do the constant energy bulk viscosities.

Table 10 Diffusion transport coefficients of model binary mixtures of model LJ Ar–CH_4 reduced units. All calculations were carried out at constant temperature, in the [*NVT*] ensemble, except the rows denoted by † which denote [*NVE*] ensemble simulations. $N = 256$. *denotes a [*NVE*] simulation with $r_c = 2.5$. The statistical uncertainty is ± 5% for the diffusion-coefficients, ± 50% for the D^T and κ_T.

x_1	ρ^*	T^*	$\rho_1 D_1$	$\rho_2 D_2$	ρD_{12}	$D^T/0.01$	k_T
0.02344	0.65382	0.83472	0.000732	0.275	0.0330	0.18	0.057
0.02344	0.65382	0.85940	0.000741	0.0285	0.0331	−0.32	−0.10†
0.20312	0.67596	0.82593	0.00650	0.0232	0.0312	0.46	0.19†
0.39844	0.70162	0.83472	0.0138	0.0188	0.0337	0.186	0.087
0.39844	0.70162	0.85513	0.0144	0.0195	0.0340	0.34	0.16†
0.39844	0.70162	0.83472	0.0138	0.0188	0.0352	−0.28	−0.127
0.60156	0.72954	0.83472	0.0223	0.0133	0.0353	−0.068	−0.037
0.60156	0.72954	0.83210	0.0220	0.0132	0.0337	−0.0025	−0.0014†
0.79687	0.75665	0.83472	0.0317	0.00731	0.0389	0.236	0.130
0.97656	0.78169	0.83472	0.0295	0.0101	0.0435	−0.10	−0.053
0.97656	0.78169	0.82855	0.0416	0.000896	0.0414	−0.078	−0.046†
0.02344	0.61042	1.0017	0.00131	0.0519	0.0571	−0.205	−0.04
0.02344	0.61042	0.9719	0.00125	0.0497	0.0543	0.38	0.073†
0.02344	0.61042	1.0822	0.00149	0.0575	0.0646	0.57	0.09†
0.39844	0.64744	1.0017	0.0246	0.0346	0.0595	0.402	0.108
0.39844	0.64744	1.0341	0.0253	0.0359	0.0658	0.075	0.018†
*0.39844	0.64744	1.0330	0.0254	0.0363	0.0610	−1.42	−0.37†
0.60156	0.66746	1.0017	0.0387	0.0241	0.0608	−0.26	−0.083
0.60156	0.66746	1.0017	0.0390	0.0243	0.0620	0.035	0.011†
0.97656	0.69710	1.0017	0.0710	0.00158	0.0690	0.01	0.004
0.97656	0.69710	1.0015	0.0710	0.00159	0.0715	0.05	0.016†

Table 8 also shows that the thermal conductivity of the Ar/CH_4 states over a range of compositions and temperatures. Here we find exceptionally good agreement beween the experiment and simulation data. The thermal conductivity decreases as the argon content is increased. The contribution of the enthalpy term to the thermal conductivity is small in practice because the magnitude of the extra terms it introduces in the definition of the thermal conductivity are numerically small at these densities.

Table 9 presents the simulation and experimental elastic moduli. Again there is good agreement between simulation and experiment for the shear modulus. This indicates that the above descrepancy between the shear viscosities of experiment and simulation can now be unambiguously attributed to the different reorientation relaxation times in the model and real methane.

In Table 10 we give the self- and mutual diffusion coefficients for the mixtures. As there is no experimental data to compare with, the results are mainly for future reference. We note however that $\rho D_{12} \approx \rho_1 D_1 + \rho_2 D_2$ to within about 10%, indicating near ideal behaviour. We also give the therodiffision coefficients. As noted elsewhere [8] these are difficult to obtain accurately by the present method.

5. CONCLUSIONS

In this report we have calculated thermodynamic data and transport properties for mixtures of binary Lennard-Jones liquids by equilibrium molecular dynamics. We

have covered a wide range of state points using a time correlation function approach to obtain the transport coefficients of some model Ar/CH_4 mixtures, for the first time using the correct definition of the heat flux, which is needed for over half of the transport coefficients. This expression uses the partial enthalpy of the two species, which were obtained from parallel constant pressure simulations at the same state points as the simulations used to compute the transport coefficients.

Most of the simulations were performed along two isotherms to compare with a previous experimental study of the dense fluid Ar–CH_4 mixtures [11]. This is a region of the phase diagram well-suited to MD as the correlation functions decay within the $\sim$ 5 psec followed in these simulations (this is a typical upper limit on the duration of the time correlation functions that can be followed with statistical certainty at these densities). Therefore the derived transport coefficients (obtained from Green-Kubo integration) are obtained free of 'long-time tails' which make such studies impractical at low density and in the region of glassy behaviour. (The temperatures are sufficiently high at these densities to exclude any such excessively viscous behaviour.)

A detailed comparison with the experimental study of Mikhailenko *et al.* [11] reveals exceptional agreement between the simulation and experimental values for the average densities of the mixtures at the mole fractions considered. The thermal conductivities and infinite frequency shear moduli are in very good agreement also. The simulated methane shear viscosity is significantly overestimated in the near-liquid states considered here. This causes the composition dependence of the viscosity to vary in the opposite direction to that of the experimental fluid (which disobeys corresponding states). Therefore the experimental shear viscosity increases on going from pure methane to pure argon, whereas the simulated viscosities manifest the opposite behaviour. The bulk viscosity shows the same qualitative difference in behaviour between simulation and experiment. The simulation bulk viscosities show a variation with composition more in line with the simulation shear viscosities, in diminishing with increasing Ar content, the reverse to experiment. We now consider the effect of temperature at fixed compostion. The experimental argon bulk viscosity increases with temperature whereas the experimental methane bulk viscosity decreases with increasing temperature. Both simulated argon and methane bulk viscosities diminish with increasing temperature. In contrast, both the simulation and experimental pure methane and argon shear viscosities diminish with increasing temperature. Therefore the temperature dependence of the simulated bulk viscosity of methane has more in common with experimental methane, than the bulk of viscosity of simulated and experimental argon.

We also calculated the species component self-diffusion and mutual diffusion coefficients, and the thermotransport coefficients for these compositions, at this stage, largely for future reference.

Perhaps the most important conclusion from this work is that the single site model for methane, while adequate for thermodynamic and certain transport coefficients, is deficient when it comes to reproducing the shear and bulk viscosities.

Acknowledgements

D.M.H. gratefully thanks *The Royal Society* for the award of a *Royal Society 1983 University Research Fellowship*. We express gratitude to the S.E.R.C. for the award of computer time on the CRAY-XMP at the University of London Computer Centre, and the RHBNC Computer Centre also for use of their computing facilities.

References

[1] P. Borgelt, C. Hoheisel and G. Stell, "Exact molecular dynamics and kinetic theory results for thermal transport coefficients of the Lennard-Jones argon fluid in a wide region of states", *Physical Rev. A*, **42**, 789 (1990).

[2] C. Hoheisel and R. Vogelsang, "Thermal transport coefficients for one- and two-component liquids from time correlation functions computed by molecular dynamics", *Comp. Phys. Rep.*, **8**, 1–70 (1988).

[3] C. Hoheisel, "Phase separation in binary nonadditive soft-sphere mixtures", *Phys. Rev. A*, **41**, 2076 (1990).

[4] J.M. Stoker and R.L. Rowley, "Molecular dynamics simulation of real-fluid mutual diffusion coefficients with Lennard-Jones potential model", *J. Chem. Phys.*, **91**, 3670–3676 (1989).

[5] M. Schoen and C. Hoheisel, "The shear viscosity of a Lennard-Jones fluid calculated by equilibrium molecular dynamics", *Mol. Phys.*, **56**, 653–672 (1985).

[6] P. Malbrunot, A. Boyer, E. Charles and H. Abachi, "Experimental bulk viscosities of argon, krypton, and xenon near their triple point", *Phys. Rev. A*, **27**, 1523–1534 (1983).

[7] R. Vogelsang, G. Hoheisel and M. Luckas, "Shear viscosity and thermal conductivity of the Lennard-Jones Liquid computed using molecular dynamics and predicted by a memory function model for a large number of states", *Mol. Phys.*, **64**, 1203–1213 (1988).

[8] R. Vogelsang and C. Hoheisel, "The Dufour and Soret coefficients of isotopic mixtures from equilibrium molecular dynamics calculations", *J. Chem. Phys.*, **89**, 1588 (1988).

[9] D.J. Evans and H.J.M. Hanley, "Viscosity of a mixture of soft-spheres", *Phys. Rev. A*, **20**, 1648 (1979).

[10] S. Murad, D.P.S. Sethi and P.V. Ravi, "Transport Properties of continuous mixtures using nonequilibrium molecular dynamics", *Fluid Phase Equilibria*, **53**, 159 (1989).

[11] S.A. Mikhailenko, B.G. Dudar and V.N. Derkach, "Viscoelastic properties and acoustic relaxation in liquid methane-argon mixtures", *Sov. J. Low Temp. Phys.*, **4**, 205 (1978).

[12] V. Vesovic and W.A. Wakeham, "Prediction of the viscosity of fluid mixtures over wide ranges of temperature and pressure", *Chem. Eng. Sci.*, **44**, 2189 (1989).

[13] I.R. McDonald, "*NPT*—ensemble Monte Carlo calculations for binary liquid mixtures", *Mol. Phys.*, **23**, 41–58 (1972).

[14] M. Nunes da Ponte, W.B. Streett, R.C. Miller and I.A.K. Stavely, "An experimental study of the equation of state of liquid (argon + methane), and the effect of pressure on their excess thermodynamic functions", *J. Chem. Thermodynamics*, **13**, 767 (1981).

[15] P. Sindzingre, C. Ciccotti, C. Massobrio and D. Frenkel, "Partial enthalpies and related quantities in mixtures from computer simulation", *Chem. Phys. Lett.*, **136**, 35–41 (1987).

[16] P. Sindzingre, C. Massobrio, G. Ciccotti, and D. Frenkel, "Calculations of Partial Enthalpies of an argon-krypton mixture by *NPT* Molecular Dynamics", **129**, 213–224 (1989).

[17] M.P. Allen and D.J. Tildesley, "Computer Simulation of Liquids" (Clarendon, Oxford, 1987).

[18] H.C. Anderson, "Molecular dynamics at constant pressure and/or temperature", *J. Chem. Phys.*, **72**, 2384 (1980).

[19] D. MacGowan and D.J. Evans, "Heat and matter transport in binary liquid mixtures", *Phys. Rev. A*, **34**, 2133–2142 (1986); "Addendum to 'Heat and matter transport in binary liquid mixtures'", *Phys. Rev. A*, **36**, 948 (1987).

[20] R. Zwanzig and R.D. Mountain, "High-frequency elastic moduli of simple fluids", *J. Chem. Phys.*, **43**, 4464–4471 (1965).

[21] J.O. Hirschfelder, C.F. Curtiss and R.B. Bird, (1954), "Molecular theory of gases and liquids", John Wiley.

[22] G.M. van Waveren, J.P.J. Michels and N.J. Trappeniers, "Molecular Dynamics simulation of CH_4 in the dense fluid phase", *Physica*, **139 & 140B**, 144 (1986).

[23] M. Luckas, M. Ripke and K. Lucas, "Prediction of the thermophysical properties of fluid methane from the SSR-MPA potential, *Fluid Phase Equil.*, **58**, 35 (1990).

[24] A.D. Simmons and P.T. Cummings, "Non-equilibrium molecular dynamics simulation of dense fluid methane", *Chem. Phys. Lett.*, **129**, 92 (1986).

[25] A.J. Easteal and L.A. Woolf, "Developments in the hard sphere model for self-diffusion and shear viscosity: Methane as a model hard sphere fluid.", *Physica B*, **124** 173 (1984).

[26] A.J. Easteal and L.A. Woolf, "Developments in the hard sphere model for self-diffusion and shear viscosity: applications based on methane as a model hard-sphere fluid", *Physica B*, **124**, 182 (1984).

[27] D.E. Diller, "Measurements of the viscosity of compressed gaseous and liquid methane", *Physica A*, **104**, 417 (1980).

[28] J.J. Van Loef and E.G.D. Cohen, "Transport Coefficients of simple fluids in a density range from the solid to the dilute gas", *Physica A*, **156**, 522 (1989).
[29] A.A. Clifford, J. Kestin and W.A. Wakeham, "Thermal conductivity of N_2, CH_4 and CO_2 at room temperature and at pressures up to 35 MPa", *Physica A*, **97**, 287 (1979).
[30] F.X. Prielmeier and H.-D. Ludemann, "Self diffusion in compressed liquid chloromethane, dichloromethane and trichloromethane", *Mol. Phys.*, **58**, 593 (1986).
[31] R. Castillo and J.V. Orozco, "The thermal conductivity of dense fluids and their mixtures using the effective diameter revised enskog theory", *Physica A*, **166**, 505 (1990).
[32] R. Castillo and S. Castaneda, "The bulk viscosity in dense fluids", *Int. J. of Thermophysics*, **9**, 383 (1990).
[33] D.M. Heyes and S.R. Preston, "Transport Coefficients of Ar–Kr Mixtures by Molecular Dynamics Computer Simulation", *Phys. Chem. Liq.* **23**, (1991) 123.